C. Giordano, G. Varga, R. Mackenzie, A. Boutonnet, F. Topputo
Target-Based Guidance Method for Trajectories with Multiple Flybys
Journal of Guidance Control and Dynamics, published online 25/01/2023
doi:10.2514/1.G006792

Target-based guidance method for trajectories with multiple flybys

Carmine Giordano*
Politecnico di Milano, Milan, Italy, 20156

Gabor Varga† and Ruaraidh Mackenzie‡ and Arnaud Boutonnet §
European Space Agency, Darmstadt, Germany, D-64293

Francesco Topputo¶
Politecnico di Milano, Milan, Italy, 20156

I. Introduction

In a real-life scenario, a spacecraft will not follow the prescribed nominal path. As a matter of fact, uncertainty in the dynamic model (e.g., gravitational parameters or radiation pressure noisy profiles) can lead to relevant drifts during ballistic arcs, while errors in command actuation (i.e., thrust magnitude and pointing angles error) can inject the spacecraft on unwanted trajectories [1]. Moreover, the spacecraft state cannot be known exactly, since it is inferred only from indirect measurements subjected to noise.

Some trajectory correction maneuvers (TCMs) are planned along the transfer to compensate for the trajectory drift and allow the spacecraft to reach the target. These tailored impulses are quantified through dedicated guidance laws. These techniques can be subdivided into two main groups: 1) Closed-loop control, if control impulses are given to track the reference guidance, or 2) Closed-loop guidance, if control impulses are given to update the whole spacecraft trajectory to satisfy the mission objectives. Moreover, the control thrust can be provided either when a certain quantity (e.g., the state knowledge) exceeds a threshold or at some prescribed epochs, provided by the on-ground flight dynamics team, and the impulse vector can be computed to control the full state or just some components. The choice of the most suitable method is based essentially on the mission profile, spacecraft characteristics, and the general scenario.

For deep space missions, closed-loop control methods are considered suitable techniques due to their robustness, easy implementation, and fast computational times. Among them, differential guidance [2, 3] is a commonly used method. It aims to cancel out position and velocity deviations with respect to the nominal trajectory at some future given time, using a single burn at the present time. Model predictive control is another popular choice for tracking a reference trajectory [4]. Recently, the increasing demand for autonomy in guidance and control lead to novel techniques able to be implemented on-board, such as machine learning [5] and sequential convex programming [6]. These two techniques

*PostDoc Fellow, Dept. of Aerospace Science and Technology; carmine.giordano@polimi.it. AIAA Member.
†Mission Analyst, HSO-GFA; gabor.varga@esa.int.
‡Senior Mission Analyst, HSO-GFA; ruaraidh.mackenzie@esa.int.
§Senior Mission Analyst, HSO-GFA; arnaud.boutonnet@esa.int.
¶Full Professor, Dept. of Aerospace Science and Technology; francesco.topputo@polimi.it. AIAA Senior Member.

were successfully applied to planetary [7] and asteroid [8] descent and landing. Special methods were designed to cope with Lagrange Points Orbits (LPOs) [9], trying to target a future state of the LPOs using an LQR-like approach [10] or trying to control the unstable directions [11, 12]. In the case of close-proximity operations around asteroids, control methods exploiting an application of generalized Zero-Effort-Miss/Zero-Effort-Velocity feedback guidance algorithm [13], using sliding control [14] or adapting intercept missile guidance to the space scenario [15] were devised.

In some mission scenarios, it can be a key element to meet targets along the trajectory, rather than catching up to a prescribed state at each correction maneuver epoch. In these cases, algorithms whose aim is to compensate for state deviations can unreasonably increase navigation costs. A notable example can be mission profiles with several back-to-back fly-bys, where hitting a precise close approach altitude is paramount, or in the case of close proximity operations about minor bodies, where achieving scientific objectives can be more stringent than reaching exact way-point passages. For this kind of trajectories, a guidance law able to fulfill prescribed engineering or scientific requirements by giving control impulses at some given times can be beneficial. For this reason, a novel concept, labeled target guidance (TG), has been devised in this note. This technique uses some impulses to compensate for the deviations from both engineering and scientific prescribed targets, instead of tracking the nominal state or recomputing the whole trajectory downstream. The goal of this note is to model the target guidance with mathematical means, to provide a method to estimate the required control impulses, and to assess its performances both in stochastic cost and errors on the targets in a relevant scenario. For this last point, the Europa science phase of the spacecraft JUICE is selected as the application case. It is characterized by several back-to-back fly-bys, separated by just a few days, and having some strict requirements on close-approach altitudes and latitudes for both scientific and engineering reasons.

The note is structured as follows. An overview of the problem at controlling a spacecraft is given in Section II. The target guidance method is introduced in Section III and the test case scenario is presented in Section V. A performance assessment for the target guidance is shown in Section V together with a comparison against the differential guidance.

II. The Spacecraft Control Problem

During a spacecraft journey, on-ground flight dynamics (FD) teams have the duty to 1) estimate the spacecraft's real state from indirect measurements (i.e., perform the navigation), and, from that, 2) compute the impulse to control the spacecraft trajectory. Usually, for interplanetary missions, flight dynamics tasks are performed following a weekly pattern in order to ease the work organization and simplify the ground stations' schedule. The flight dynamics team routine can be modeled into three phases (Fig. 1):

1) *orbit determination (OD) phase*, where measurements, e.g., range and range-rate, are collected and prepared to be fed into an estimation filter [16]. This phase ends at the cut-off time, that is the time-tag of the final navigation data to be used in the filter.;
2) *cut-off phase*, in which the spacecraft state is estimated and the control impulse is computed. At the end of this

phase, the control impulse is uploaded to the spacecraft, then performed at the expected epoch;

3) *ballistic phase*, where the spacecraft follows an unobserved, uncontrolled trajectory.

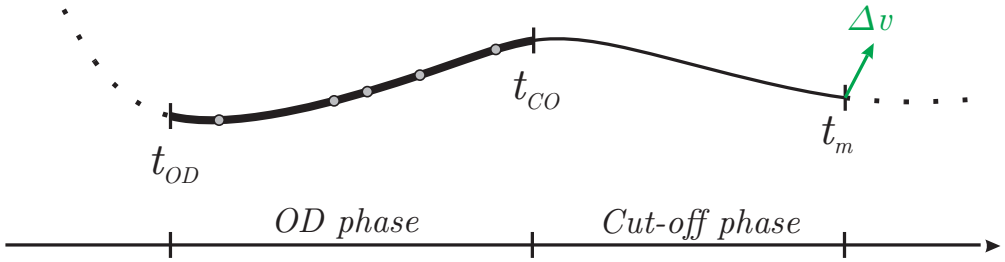

Fig. 1 Flight dynamics team routine timeline with the ballistic phase indicated with a dotted line and the measurement times as dots.

It is important to note that the last measurement is taken at t_{CO}, that is hours, or even days, before the application of the control maneuver. This cut-off time is needed by the on-ground team to perform FD duties, validate the results, and prepare and send telecommands to the spacecraft. Moreover, the TCMs are computed considering the estimated state at t_m, that is the output of the OD process, since the real state cannot be known exactly from the ground.

Remark 1. The spacecraft control problem can be summarized as: Starting from the estimated trajectory data, collected from time t_{OD} up to time t_{CO}, find the control impulses $\Delta\mathbf{v}$ to be given at the prescribed time t_m to allow the spacecraft to reach the desired targets.

III. Mathematical Formulation

For illustration purposes, a spacecraft flying a trajectory having a single required target at a given time t_T is considered. The spacecraft performs M trajectory correction maneuvers at some prescribed times $\{t_1, \ldots, t_k, \ldots t_M\} \in [t_0, t_T]$ (Fig. 2). At the initial time t_0, the nominal state is indicated with $\mathbf{x}_0^*$, while the real state is $\mathbf{x}_0$.

Assuming that the time interval between navigation maneuvers is relatively short and, thus, the real trajectory does not significantly drift from the nominal one, first-order (linear) approximation can be used to relate the initial and final deviations. Hence, the pre-maneuver state (indicated with a superscript -) at the first trajectory correction maneuver time t_1 can be computed as

$$\mathbf{x}_1^- = \mathbf{x}_1^* + \Phi\left(t_0, t_1\right)\delta\mathbf{x}_0 \tag{1}$$

where indexes correlate to TCM epochs, $\Phi\left(t_0, t_1\right)$ is the state transition matrix (STM) from t_0 to t_1, i.e., $\Phi = \partial\mathbf{x}_1^*/\partial\mathbf{x}_0^*$, and $\delta\mathbf{x}_0$ is the state deviation at the initial time t_0. Its value can be defined as

$$\delta\mathbf{x}_0 = \mathbf{x}_0 - \mathbf{x}_0^* \tag{2}$$

In a real-life situation, $\mathbf{x}_0$ is conveniently substituted by its estimated value.

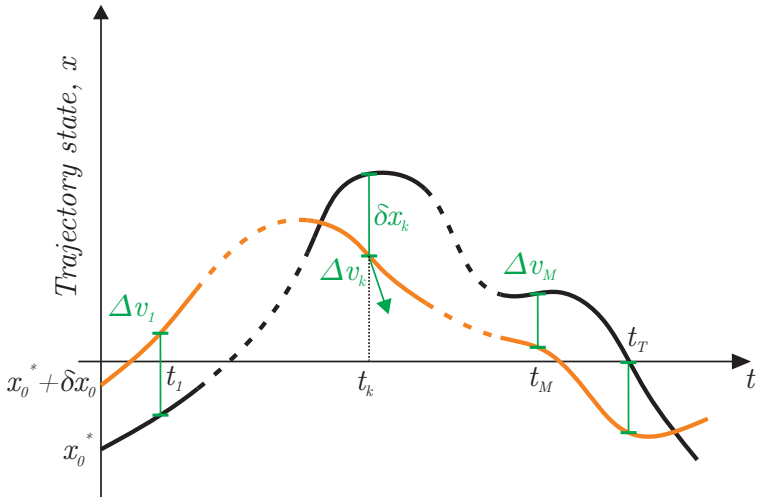

Fig. 2 Target Guidance concept, with the nominal path as a black line and the real trajectory as an orange line.

After applying the correction maneuver, the post-maneuver real state, marked with a superscript +, reads

$$\mathbf{x}_1^+ = \mathbf{x}_1^* + \underbrace{\Phi\left(t_0, t_1\right)\delta\mathbf{x}_0 + \begin{bmatrix}\mathbf{0}\\ \Delta v_1\end{bmatrix}}_{\delta\mathbf{x}_1} \tag{3}$$

with $\delta\mathbf{x}_1$ indicating the post-maneuver deviation with respect to the nominal state at t_1. If this deviation is propagated forward to the second correction epoch t_2, the state is

$$\mathbf{x}_2^- = \mathbf{x}_2^* + \Phi\left(t_1, t_2\right)\delta\mathbf{x}_1 = \mathbf{x}_2^* + \Phi\left(t_1, t_2\right)\left(\Phi\left(t_0, t_1\right)\delta\mathbf{x}_0 + \begin{bmatrix}\mathbf{0}\\ \Delta v_1\end{bmatrix}\right) = \mathbf{x}_2^* + \Phi\left(t_0, t_2\right)\delta\mathbf{x}_0 + \Phi\left(t_1, t_2\right)\begin{bmatrix}\mathbf{0}\\ \Delta v_1\end{bmatrix} \tag{4}$$

where the composition property for the STM, i.e., $\Phi\left(t_1, t_2\right)\Phi\left(t_0, t_1\right) = \Phi\left(t_0, t_2\right)$, has been exploited. This procedure can be applied recursively up to a generic TCM time t_k, leading to

$$\mathbf{x}_k^+ = \mathbf{x}_k^* + \underbrace{\Phi_0^k\delta\mathbf{x}_0 + \sum_{i=1}^{k}\Phi_i^k I_v \Delta v_i}_{\delta\mathbf{x}_k} \tag{5}$$

where $\delta\mathbf{x}_k$ is the post-maneuver deviation, $\Phi_{j-1}^j = \Phi(t_{j-1}, t_j)$ and $I_v = [0_3, I_3]^T$ is a (6×3)-dimensional block matrix, able to extract the 3-by-3 bottom-right part of the STM. Under this framework, the target state (at time t_T) can be written

as

$$\mathbf{x}_T = \mathbf{x}_T^* + \underbrace{\Phi(t_k, t_T)\delta\mathbf{x}_M}_{\delta\mathbf{x}_T} \tag{6}$$

where $\delta\mathbf{x}_M$ is the post-maneuver state deviation with respect to nominal trajectory at t_M (i.e., the last TCM time before the target), computed through Eq. (5).

The *target function* f is defined as the function that must be zero at time t_t to fulfill the mission objective. For example, if the target is a desired latitude ℓ_δ with respect to the central body at the close approach, the target function should be defined as $f(\mathbf{x}_T) = \ell(t_T) - \ell_\delta$. The first-order expansion of f is

$$f(\mathbf{x}_T) \simeq \cancelto{0}{f\left(\mathbf{x}_T^*\right)} + \left.\frac{\mathrm{d}f}{\mathrm{d}\mathbf{x}}\right|_{\mathbf{x}_T^*} \delta\mathbf{x}_T = 0 \tag{7}$$

since $f\left(\mathbf{x}_T^*\right)$ is zero by definition. Substituting Eq. (5) in Eq. (6), and in turn in Eq. (7),

$$f(\mathbf{x}_T) \simeq \left.\frac{\mathrm{d}f}{\mathrm{d}\mathbf{x}}\right|_{\mathbf{x}_T^*} \Phi_M^T \left(\Phi_0^M \delta\mathbf{x}_0 + \sum_{i=1}^{M} \Phi_i^M I_v \Delta v_i\right) = \left.\frac{\mathrm{d}f}{\mathrm{d}\mathbf{x}}\right|_{\mathbf{x}_T^*} \Phi_0^T \delta\mathbf{x}_0 + \left.\frac{\mathrm{d}f}{\mathrm{d}\mathbf{x}}\right|_{\mathbf{x}_T^*} \sum_{i=1}^{M} \Phi_i^T I_v \Delta v_i = 0 \tag{8}$$

Assuming that f is known and it is at least a C^1-class function, i.e., a differentiable function whose first derivative is continuous, Eq. (8) can be written in compact form as

$$A_0 \delta\mathbf{x}_0 + A\boldsymbol{\Delta v} = 0 \tag{9}$$

where $A_0 = \left.\frac{\partial f}{\partial \mathbf{x}}\right|_{\mathbf{x}_T^*} \Phi_0^T$ and $A = \left.\frac{\partial f}{\partial \mathbf{x}}\right|_{\mathbf{x}_T^*} \sum_{i=1}^{M} \Phi_T^i I_v$, and

$$\boldsymbol{\Delta v} = \begin{bmatrix} \Delta v_1 \\ \Delta v_2 \\ \vdots \\ \Delta v_M \end{bmatrix}$$

The algorithm can be modified for a multi-dimensional target function. In this case, matrices A_0 and A should be modified accordingly, that is

$$A_0 = \frac{\mathrm{d}f_i}{\mathrm{d}\mathbf{x}_0^*} = \begin{bmatrix} \frac{\mathrm{d}f_1}{\mathrm{d}\mathbf{x}_0^*} \\ \vdots \\ \frac{\mathrm{d}f_N}{\mathrm{d}\mathbf{x}_0^*} \end{bmatrix} \in \mathbb{R}^{N\times 6} \tag{10}$$

while A is

$$A = \frac{\mathrm{d}f_i}{\mathrm{d}\Delta v_k} = \begin{bmatrix} \frac{\mathrm{d}f_1}{\mathrm{d}\Delta v_1} & \mathbf{0}_3 & \dots & \mathbf{0}_3 \\ \frac{\mathrm{d}f_2}{\mathrm{d}\Delta v_1} & \frac{\mathrm{d}f_2}{\mathrm{d}\Delta v_2} & \dots & \mathbf{0}_3 \\ \vdots & \vdots & \ddots & \vdots \\ \frac{\mathrm{d}f_N}{\mathrm{d}\Delta v_1} & \frac{\mathrm{d}f_N}{\mathrm{d}\Delta v_2} & \dots & \frac{\mathrm{d}f_N}{\mathrm{d}\Delta v_M} \end{bmatrix} \in \mathbb{R}^{N\times(3M)} \tag{11}$$

where N is the number of target functions, while M the number of control maneuvers. Zeros in Eq. (11) are related to the fact that impulses future in time cannot modify the trajectory in the past.

Moreover, a *target-trigger function* g is introduced. It is an equality constraint that shall be null whenever the target condition specified in the function f is reached. Thus, it checks that the target is happening at the right moment. For example, considering as target a desired latitude λ_δ at the close approach, the target trigger function will be the close approach condition, i.e., $g = (\mathbf{r}\cdot\mathbf{v}) = 0$. Considering a linear expansion,

$$g\left(\mathbf{x}_T\right) \simeq \cancelto{0}{g\left(\mathbf{x}_T^*\right)} + \left.\frac{\mathrm{d}g}{\mathrm{d}\mathbf{x}}\right|_{\mathbf{x}_T^*} \delta\mathbf{x}_T = 0 \tag{12}$$

Repeating mathematical steps of Eqs. (8)–(9), assuming g is a known C^1-class function, Eq. (12) is simplified as

$$G_0\delta\mathbf{x}_0 + G\boldsymbol{\Delta v} = 0 \tag{13}$$

An optimization problem is set in order to minimize the sum of the stochastic cost, i.e., the sum of all the control maneuvers, while satisfying the targeting constraints given by Eqs. (9) and (13).

Remark 2. The target guidance problem consists of finding $\Delta v_k,\ k = \{1,\dots,M\}$, such that

$$J = \sum_{k=1}^{M} \frac{1}{2}\left\|\Delta v_k\right\|^2 = \frac{1}{2}\boldsymbol{\Delta v}^T\boldsymbol{\Delta v} \tag{14}$$

is minimized, subjected to

$$\underbrace{\begin{bmatrix} A \\ G \end{bmatrix}}_{B} \boldsymbol{\Delta v} = -\underbrace{\begin{bmatrix} A_0 \\ G_0 \end{bmatrix}}_{B_0} \delta\mathbf{x}_0 \tag{15}$$

Applying the Lagrange theory [17], the Lagrange function associated to the optimization problem is

$$\mathcal{L} = \frac{1}{2}\boldsymbol{\Delta v}^T\boldsymbol{\Delta v} + \boldsymbol{\lambda}^T\left(B\boldsymbol{\Delta v} + B_0\delta\mathbf{x}_0\right) \tag{16}$$

where $\boldsymbol{\lambda}$ is the Lagrange multipliers vector. In this case, the necessary condition for the optimization problem are

$$\begin{cases} \dfrac{\partial \mathcal{L}}{\partial \boldsymbol{\Delta v}} = \boldsymbol{\Delta v} + B^T \boldsymbol{\lambda} = \mathbf{0} \\ \dfrac{\partial \mathcal{L}}{\partial \boldsymbol{\lambda}} = B\boldsymbol{\Delta v} + B_0 \delta \mathbf{x}_0 = \mathbf{0} \end{cases} \tag{17}$$

The two conditions in Eq. (17) can be written in a more elegant compact form

$$\begin{bmatrix} I_{3M} & B^T \\ B & 0_{2N} \end{bmatrix} \begin{bmatrix} \boldsymbol{\Delta v} \\ \boldsymbol{\lambda} \end{bmatrix} = - \begin{bmatrix} \mathbf{0}_{3M} \\ B_0 \delta \mathbf{x}_0 \end{bmatrix} \tag{18}$$

where I_{3M} is the $3M$-dimensional identity matrix and 0_{2N} the $(2\mathrm{N} \times 2\mathrm{N})$ null matrix. Applying the explicit inverse formula for a 2×2 Hermitian block triangular matrix [18], it is possible to write

$$\begin{bmatrix} \boldsymbol{\Delta v} \\ \boldsymbol{\lambda} \end{bmatrix} = - \begin{bmatrix} I_{3M} & B^T \\ B & 0_{2N} \end{bmatrix}^{-1} \begin{bmatrix} \mathbf{0}_{3M} \\ B_0 \delta \mathbf{x}_0 \end{bmatrix} = - \begin{bmatrix} I_{3M} - B^T \left(BB^T\right)^{-1} B & B^T \left(BB^T\right)^{-1} \\ \left(BB^T\right)^{-1} B & -\left(BB^T\right)^{-1} \end{bmatrix} \begin{bmatrix} \mathbf{0}_{3M} \\ B_0 \delta \mathbf{x}_0 \end{bmatrix} \tag{19}$$

Taking the first row of Eq. (19), the optimal impulses can be expressed as

$$\boldsymbol{\Delta v} = -B^T \left(BB^T\right)^{-1} B_0 \delta \mathbf{x}_0 = -B^\dagger B_0 \delta \mathbf{x}_0 \tag{20}$$

where $B^\dagger$ is the Moore–Penrose pseudo-inverse matrix of B [19].

Note that this system is well-posed only if $3M \geq 2N$; hence, at least 2 trajectory correction maneuvers are needed to match 3 scalar targets. This method can be applied in a receding horizon approach, meaning that, $\delta \mathbf{x}_0$, B, and B_0 are updated at some prescribed times, a new value for the whole vector $\boldsymbol{\Delta v}$ is computed, but only the first Δv_k is applied in practice, while the others are recomputed again in the subsequent legs. Moreover, it is important to notice that the algorithm computes TCMs able to control all target states downstream. This characteristic is of paramount importance whenever several targets close in time are selected.

In the formulation presented in this section, the target times are considered to be fixed. This choice allows to have a fixed plan for the scientific payloads. However, it is expected that the performances would improve if target times are left free to vary. In this case, the decision variable vector will be extended with a N-dimensional vector δt_T, representing the difference of the optimized target times from the nominal ones, while Eqs. (7) and (12) will be modified considering also the expansion of f and g with respect the target time t_T.

IV. Test case scenario

In order to assess the performances of the target guidance, a test in a relevant scenario has been performed. The European Space Agency (ESA) mission Jupiter Icy Moon Explorer (JUICE) [20], planning to perform a tour of the Jovian system, is considered. JUICE is an interplanetary mission, developed by ESA, having the aim to study three of the Galilean Jupiter moons, namely Ganymede, Callisto, and Europa. At the time this work has been performed, the spacecraft is planned to be launched in 2022 and it will reach Jupiter in 2029. A tour of the Jovian moons is foreseen, having the twofold aim to change the spacecraft trajectory by reducing its energy and then increasing the inclination by exploiting several Callisto fly-bys, and to perform scientific observation during the close approaches. The tour ends in 2032 when the spacecraft is inserted on a elliptic orbit about Ganymede.

In this work, the focus is placed on the Europa scientific phase [21]. It consists of two close approaches with Europa, preceded by a close encounter with Ganymede and followed by a fly-by of Callisto. Between the first and the second Europa swing-by, a deterministic maneuver, tagged as EU1, is performed in order to prepare the spacecraft for the second encounter about Europa. This leg is summarized in Table 1. The label used for the fly-bys is nXm, where n is a total progressive number, X the initial of the moon name, and m a progressive number referred to the only moon X.

Table 1 Europa scientific phase summary.

Label	**Epoch**	**C/A altitude [km]**	v_∞ **[km/s]**	**C/A long. [deg]**	**C/A lat. [deg]**	Δv **[m/s]**
Start	01 SEP 2030	–	–	–	–	–
5G5	03 SEP 2030	1282	6.5	273	-3	–
6E1	17 SEP 2030	403	3.7	188	-47	–
EU1	19 SEP 2030	–	–	–	–	19.452
7E2	01 OCT 2030	403	3.7	179	47	–
8C1	13 OCT 2030	412	5	108	0	–
End	15 OCT 2030	–	–	–	–	–
Total	45 d					19.452

Spacecraft dynamics are integrated in a Jupiter-centered inertial reference frame, considering the gravitational forces given by the Sun, Jupiter and the four Galilean moons. The first zonal term of Jupiter non-spherical gravity model is also taken into account. Table 2 summarizes the parameters used in the dynamical model. The state of the moons with respect to Jupiter are retrieved from the IMCCE ephemeris file [22].

Gaussian uncertainties related both to navigation and command errors are considered. Navigation errors are taken into account as state deviations at the end of the OD phase. A smaller error is considered in the spacecraft–Earth radial direction, while higher errors are considered in the track and cross-track directions, since navigation rely mainly on range and range-rate measurements with Earth facilities. Uncertainty in modulus and direction associated to the deterministic maneuver is put in the loop in order to increase the model reliability. The initial dispersion (i.e., the deviation of the real trajectory from the nominal) is modeled as a Gaussian random variable, centered at the nominal

Table 2 Parameters for the JUICE dynamical model.

Body	Parameter	Value
Jupiter	μ	$126\,686\,534\,\mathrm{km}^3/\mathrm{s}^2$
	J_2	0.014735
Europa	μ	$3202.73\,\mathrm{km}^3/\mathrm{s}^2$
Ganymede	μ	$9887.83\,\mathrm{km}^3/\mathrm{s}^2$
Callisto	μ	$7179.29\,\mathrm{km}^3/\mathrm{s}^2$
Io	μ	$5959.92\,\mathrm{km}^3/\mathrm{s}^2$

state. In conclusion, 57 uncertainties affect Europa phase for JUICE. Table 3 contains the uncertainty characteristics.

Table 3 Standard deviation of JUICE uncertainty. r_0 and v_0 indicates the initial state, Δv and δ are the maneuver magnitude and direction. r, t and c stay for radial, track and cross-track measurement errors.

σ_{r_0} [km]	σ_{v_0} [m/s]	$\sigma_{\Delta v}$ [%]	σ_δ [deg]
5	0.01	1	0.5
σ_r [km]	$\sigma_{t,c}$ [km]	σ_{v_r} [mm/s]	$\sigma_{v_{t,c}}$ [mm/s]
1	4	1	4

FD tasks are expected to follow a weekly schedule to ease the on-ground team organization. However, in order to minimize the possible trajectory errors related to incorrect fly-bys, an OD session is placed three days before each close approach, and another OD session is scheduled to happen 5 days after each fly-bys in order to correct as soon as possible the state deviations related to imprecise swing-bys. A cut-off time of 2 days before each TCM is enforced. All these hypotheses are reported in Table 4. From these navigation assumptions, a timeline can be inferred and it is reported in Fig. 3.

Table 4 JUICE navigation assumptions during Europa phase.

Parameter	Value
Last TCM before C/A	3 days
First OD after C/A	5 days
Cut-off time	2 days
Duty-cycle	7 days

V. Results

The analysis presented in the remainder of this section has been conducted by using the Generic Orbit Determination and Optimisation Tool (GODOT)* [23], a software under development by Mission Analysis and Flight Dynamics Sections at ESOC. GODOT is planned to be used for mission analysis at ESA as well as for operations of space probes.

*https://godot.io.esa.int/docs/ (Last retrieved on January 31, 2022)

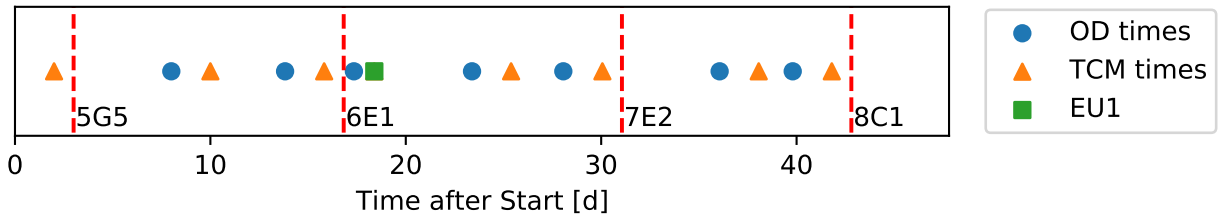

Fig. 3 Juice timeline in the Europa phase with the fly-bys times as dashed lines.

For the target guidance, it is firstly necessary to define the targets to be satisfied along the trajectory. Having several back-to-back fly-bys, it is of paramount importance to precisely target the *close approach altitudes* in order to have the post-fly-by states as close as possible to the their nominal value. Moreover, a target on the *close approach latitude* is inserted during the first Europa gravity assist, in order to fulfill the scientific need to observe in detail some surface features (namely, Thera Macula and Thrace Macula) to evaluate the presence of biosignatures. Following these consideration, the target functions f and the target trigger functions g, implemented in the target guidance algorithm, can be stated and are listed in Table 5. Once the functions associated to the desired targets are built, the matrices B and B_0 (Eq. (20)) are evaluated thought GODOT automatic differentiation routine.

Table 5 Target guidance functions for JUICE scenario, with subscripts correlating to Jupiter's moons, and ℓ a map computing the latitude given the position.

Label	**Target function** (f)	**Target trigger function** (g)
5G5 C/A altitude	$\|\mathbf{r}(t_{5G5}) - \mathbf{r}_G\| - 1282\,\text{km} = 0$	$(\mathbf{r}(t_{5G5}) - \mathbf{r}_G) \cdot (\mathbf{v}(t_{5G5}) - \mathbf{v}_G) = 0$
6E1 C/A altitude	$\|\mathbf{r}(t_{6E1}) - \mathbf{r}_E\| - 403\,\text{km} = 0$	$(\mathbf{r}(t_{6E1}) - \mathbf{r}_E) \cdot (\mathbf{v}(t_{6E1}) - \mathbf{v}_E) = 0$
6E1 C/A latitude	$\ell(\mathbf{r}(t_{6E1})) - (-47\,\text{deg}) = 0$	
6E2 C/A altitude	$\|\mathbf{r}(t_{6E2}) - \mathbf{r}_E\| - 403\,\text{km} = 0$	$(\mathbf{r}(t_{6E2}) - \mathbf{r}_E) \cdot (\mathbf{v}(t_{6E2}) - \mathbf{v}_E) = 0$
7C1 C/A altitude	$\|\mathbf{r}(t_{7C1}) - \mathbf{r}_C\| - 412\,\text{km} = 0$	$(\mathbf{r}(t_{7C1}) - \mathbf{r}_C) \cdot (\mathbf{v}(t_{7C1}) - \mathbf{v}_C) = 0$

A Monte Carlo simulation with $N = 1000$ samples was set up to perform the target guidance assessment. The number of samples was selected to have a (a-posteriori) 95% confidence level for the stochastic costs lower than 1 cm/s. Stochastic cost results are presented in Figs. 4 and 5. They show that the 95% percentile, a common measure for the stochastic costs, is about 0.5 m/s. Figs. 6 and 7 shows, as an example, the distribution of two targets error, namely the latitude at the first Europa encounter and the altitude at the second Europa fly-by. As expected, the error distributions resemble a Gaussian probability distribution function. In both cases, the mean is close to zero, while the variance is within the 0.5% level of the nominal value. A condensed summary of all the stochastic results related to the target guidance can be found in Tables 6 and 7.

In order to properly assess the performances of the target guidance, a similar Monte Carlo analysis is performed exploiting the differential guidance as control law and then results are compared. Differential guidance [3] is a well

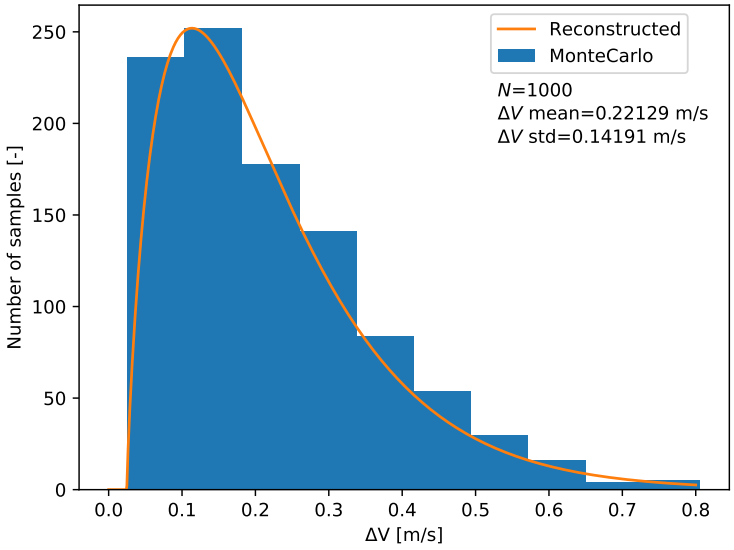

Fig. 4 Probability distribution function for the stochastic costs using target guidance, with a reconstruction using the gamma distribution.

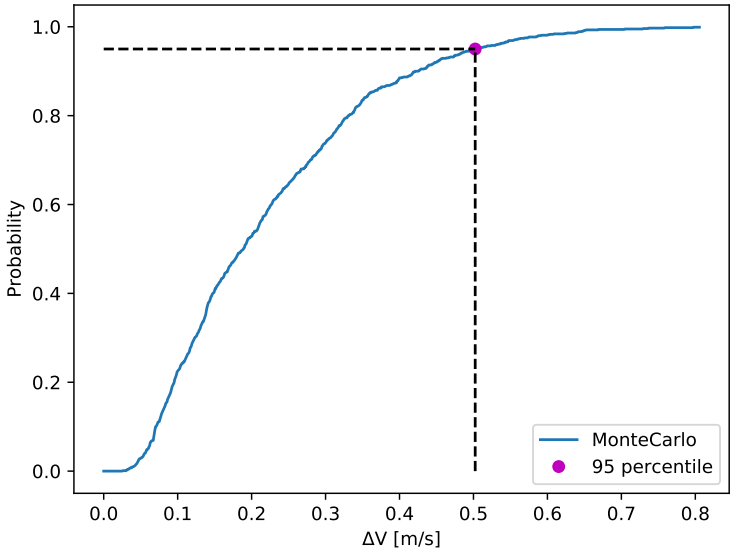

Fig. 5 Cumulative distribution function for the stochastic costs using target guidance.

established technique for deep-space closed-loop control. In this case, the control impulse is computed as

$$\Delta\mathbf{v}_k = -\left(\Phi_{rv}^T\Phi_{rv} + q\Phi_{vv}^T\Phi_{vv}\right)^{-1}\left(\Phi_{rv}^T\Phi_{rr} + q\Phi_{vv}^T\Phi_{vr}\right)\delta\mathbf{r}_k - \delta\mathbf{v}_k \tag{21}$$

where Φ_{rr}, Φ_{rv}, Φ_{vr}, and Φ_{vv} are the 3-by-3 blocks of $\Phi(t_k, t_{k+1})$, i.e., the STM associated to the nominal trajectory between two consecutive TCM times, and q is a parameter used either to adjust dimensions or the change the guidance algorithm behavior, favoring position deviation at the expense of velocity deviation and vice versa. Considering OD

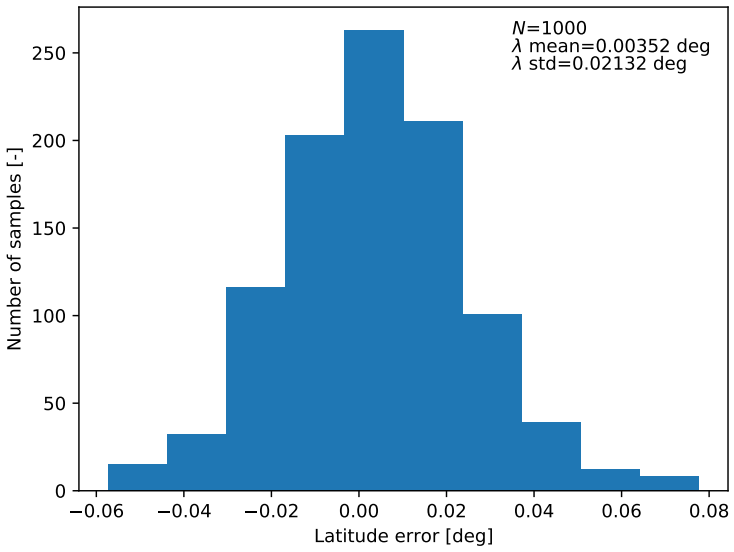

Fig. 6 Distribution error for the close-approach latitude at 6E1.

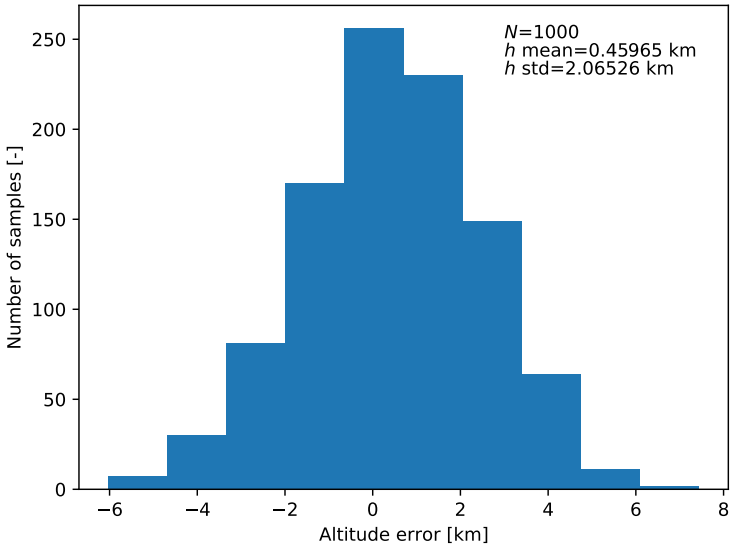

Fig. 7 Distribution error for the close-approach altitude at 7E2.

in the loop, $\delta\mathbf{r}$ and $\delta\mathbf{v}$ are the deviations with respect to the estimated trajectory. Differential guidance has already been tested for the trajectory control of JUICE and it has shown good results in terms both of costs and constraints, comparable with the ones of a full re-optimization of the trajectory [24]. Results for the stochastic costs are reported in Fig. 8 and 9. In this case, the 95% quantile is about 0.57 m/s, that is more than the 10% more expensive with respect to the target guidance. A recap for the stochastic cost comparison is given in Table 6. Targets errors are summarized in Table 6 together with a comparison with target guidance results. Although the error on the targets, measured as the central 95%-interval of the probability distribution, is always within the 2% of the nominal value, target guidance is able

to give lower errors and to reduce them up to a 5%.

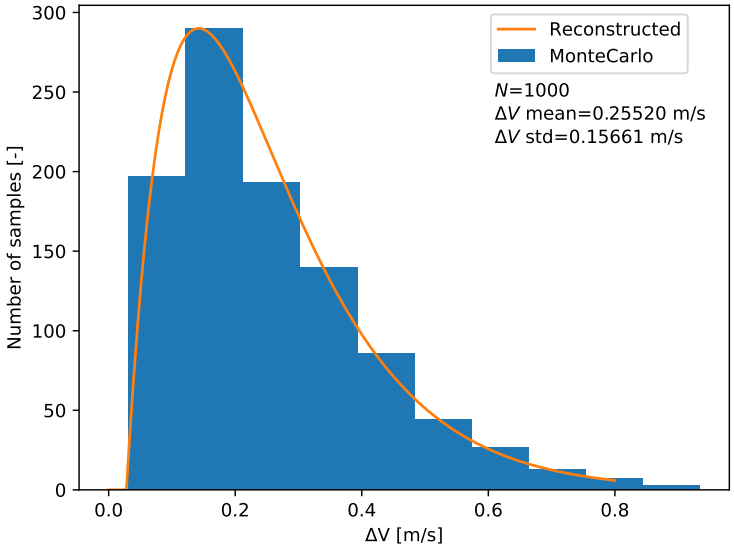

Fig. 8 Probability distribution function for the stochastic costs using differential guidance, with a reconstruction using the gamma distribution.

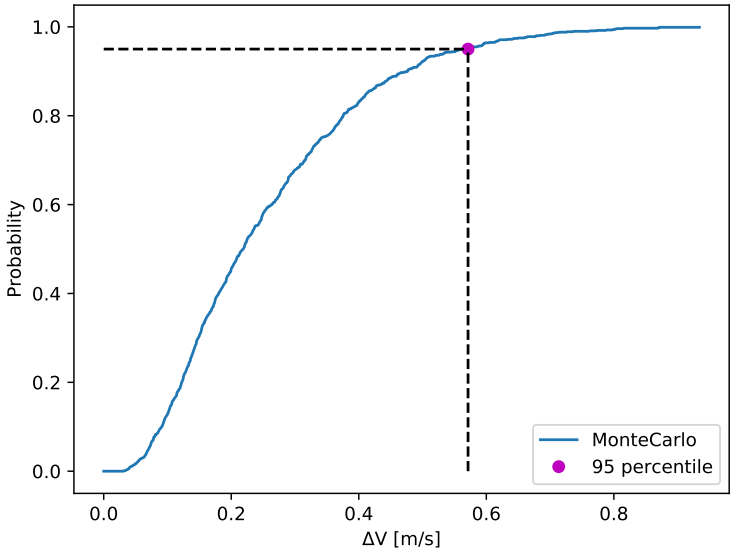

Fig. 9 Cumulative distribution function for the stochastic costs using differential guidance.

Table 6 Stochastic cost statistics summary.

Guidance algorithm	$\mu(\Delta v)$ [m/s]	$\sigma(\Delta v)$ [m/s]	95-th percentile [m/s]
Target guidance	0.22129	0.14191	0.50234
Differential guidance	0.25520	0.15661	0.57134

Table 7 Summary for the target error statistics, where white background is used for target guidance results and gray background for differential guidance.

Target	Nominal value	μ	σ	[2.5-th, 97.5-th] percentile
5G5 C/A altitude	1282 km	-0.24385 km	5.76054 km	[-13.205, 12.724] km
		-0.25408 km	5.81081 km	[-13.328, 12.825] km
6E1 C/A altitude	403 km	0.11525 km	1.44232 km	[-3.1300, 3.3605] km
		0.17838 km	1.51060 km	[-3.2210, 3.5772] km
6E1 C/A latitude	-47 deg	0.00352 deg	0.02132 deg	[-0.0444, 0.0515] deg
		0.00240 deg	0.05614 deg	[-0.1239, 0.1287] deg
7E2 C/A altitude	403 km	0.45965 km	2.06526 km	[-4.1872, 5.1065] km
		0.62363 km	2.13067 km	[-4.1704, 5.4176] km
8C1 C/A altitude	412 km	0.01422 km	1.88542 km	[-4.2280, 4.2564] km
		-0.00495 km	1.90203 km	[-4.2845, 4.2746] km

VI. Conclusions

In this work, a novel closed-loop control algorithm, labeled target guidance, is devised. Its approach is based on the definition of some targets that should be satisfied along the spacecraft trajectory, rather than catching the nominal full state. Even though, the construction of the control matrices can require an additional effort, target guidance is able to reduce the stochastic costs of more than a 10% with respect to the differential guidance, while keeping the errors on the prescribed targets within a 2% of the nominal value. Its use when hitting intermediate targets is more important than tracking the reference state can be beneficial and can bring to significant reduction in the stochastic cost.

Acknowledgments

C.G. would like to acknowledge the funding received from the European Union under the Erasmus+ program.

References

[1] Fehse, W., *Automated Rendezvous and Docking of Spacecraft*, Cambridge University Press, 2003, Vol. 16, pp. 79–80. https://doi.org/10.1017/CBO9780511543388.

[2] Park, R. S., and Scheeres, D. J., "Nonlinear Mapping of Gaussian Statistics: Theory and Spplications to Dpacecraft Trajectory Design," *Journal of Guidance, Control, and Dynamics*, Vol. 29, No. 6, 2006, pp. 1367–1375. https://doi.org/10.2514/1.20177.

[3] Dei Tos, D. A., Rasotto, M., Renk, F., and Topputo, F., "LISA Pathfinder mission extension: A feasibility analysis," *Advances in Space Research*, Vol. 63, No. 12, 2019, pp. 3863–3883. https://doi.org/10.1016/j.asr.2019.02.035.

[4] Huang, R. C., Hwang, I., and Corless, M. J., "Nonlinear Algorithm for Tracking Interplanetary Low-Thrust Trajectories," *Journal of Guidance, Control, and Dynamics*, Vol. 35, No. 2, 2012, pp. 696–700. https://doi.org/10.2514/1.53001.

[5] LaFarge, N. B., Miller, D., Howell, K. C., and Linares, R., "Autonomous closed-loop guidance using reinforcement learning

in a low-thrust, multi-body dynamical environment," *Acta Astronautica*, Vol. 186, 2021, pp. 1–23. https://doi.org/10.1016/j.actaastro.2021.05.014.

[6] Hofmann, C., and Topputo, F., "Rapid Low-Thrust Trajectory Optimization in Deep Space Based on Convex Programming," *Journal of Guidance, Control, and Dynamics*, Vol. 44, No. 7, 2021, pp. 1379–1388. https://doi.org/10.2514/1.G005839.

[7] Furfaro, R., Scorsoglio, A., Linares, R., and Massari, M., "Adaptive generalized ZEM-ZEV feedback guidance for planetary landing via a deep reinforcement learning approach," *Acta Astronautica*, 2020. https://doi.org/j.actaastro.2020.02.051.

[8] Yang, H., Bai, X., and Baoyin, H., "Rapid Generation of Time-Optimal Trajectories for Asteroid Landing via Convex Optimization," *Journal of Guidance, Control, and Dynamics*, Vol. 40, No. 3, 2017, pp. 628–641. https://doi.org/10.2514/1.G002170.

[9] Shirobokov, M., Trofimov, S., and Ovchinnikov, M., "Survey of Station-Keeping Techniques for Libration Point Orbits," *Journal of Guidance, Control, and Dynamics*, Vol. 40, No. 5, 2017, pp. 1085–1105. https://doi.org/10.2514/1.G001850.

[10] Dei Tos, D. A., and Baresi, N., "Genetic optimization for the orbit maintenance of libration point orbits with applications to EQUULEUS and LUMIO," *AIAA Scitech 2020 Forum*, Orlando, FL, 2020. https://doi.org/10.2514/6.2020-0466.

[11] Simó, C., Gómez, G., Llibre, J., Martinez, R., and Rodriguez, J., "On the optimal station keeping control of halo orbits," *Acta Astronautica*, Vol. 15, No. 6-7, 1987, pp. 391–397. https://doi.org/10.1016/0094-5765(87)90175-5.

[12] Howell, K. C., and Keeter, T. M., "Station-Keeping Strategies for Libration Point Orbits: Target Point and Floquet Mode Approaches," *AIAA/AAS Spaceflight Mechanics Meeting*, Albuquerque, New Mexico, 1995, pp. 1377–1396.

[13] Guo, Y., Hawkins, M., and Wie, B., "Applications of Generalized Zero-Effort-Miss/Zero-Effort-Velocity Feedback Guidance Algorithm," *Journal of Guidance, Control, and Dynamics*, Vol. 36, No. 3, 2013, pp. 810–820. https://doi.org/10.2514/1.58099.

[14] Furfaro, R., "Hovering in Asteroid Dynamical Environments Using Higher-Order Sliding Control," *Journal of Guidance, Control, and Dynamics*, Vol. 38, No. 2, 2015, pp. 263–279. https://doi.org/10.2514/1.G000631.

[15] Kawaguchi, J., Hashimoto, T., Kubota, T., Sawai, S., and Fujii, G., "Autonomous optical guidance and navigation strategy around a small body," *Journal of Guidance, Control, and Dynamics*, Vol. 20, No. 5, 1997, pp. 1010–1017. https://doi.org/10.2514/2.4148.

[16] Schutz, B., Tapley, B., and Born, G. H., *Statistical orbit determination*, Elsevier, 2004, Chaps. 1–3.

[17] Longuski, J. M., Guzmán, J. J., and Prussing, J. E., *Optimal Control with Aerospace Applications*, Springer, 2014, pp. 4–6. https://doi.org/10.1007/978-1-4614-8945-0.

[18] Lu, T.-T., and Shiou, S.-H., "Inverses of 2× 2 block matrices," *Computers & Mathematics with Applications*, Vol. 43, No. 1-2, 2002, pp. 119–129. https://doi.org/10.1016/S0898-1221(01)00278-4.

[19] Petersen, K. B., and Pedersen, M. S., *The Matrix Cookbook*, Technical University of Denmark, 2012. URL https://www.math.uwaterloo.ca/~hwolkowi/matrixcookbook.pdf.

[20] Boutonnet, A., and Schoenmaekers, J., "Mission Analysis for the JUICE Mission," *Advances in the Astronautical Sciences*, Vol. 143, 2012, pp. 1561–1578.

[21] Boutonnet, A., and Varga, G., "JUICE Equinox Jupiter Tour: the Challenge of Long Eclipses," *Advances in the Astronautical Sciences*, Vol. 168, 2019, pp. 3139–3149.

[22] Lainey, V., Arlot, J.-E., Karatekin, Ö., and Van Hoolst, T., "Strong tidal dissipation in Io and Jupiter from astrometric observations," *Nature*, Vol. 459, No. 7249, 2009, pp. 957–959. https://doi.org/10.1038/nature08108.

[23] The GODOT team at ESA/ESOC, "GODOT (Generic Orbit Determination and Optimisation Toolkit)," ver. 0.7.0, Last retrieved: 2022-01-31. URL https://gitlab.space-codev.org/godot.

[24] Gastaldello, N., "Preliminary Navigation Analysis for the Flyby Tour of ESA's JUICE mission: An investigation on the trajectory correction maneuvers design," Master's thesis, TU Delft, 2016. URL http://resolver.tudelft.nl/uuid:455ec2e9-a36b-445c-a9ae-ef6acbbf58f8.